

PAPER • OPEN ACCESS

Influence of tin oxide decoration on the junction conductivity of silver nanowires

To cite this article: Lilian Maria Vogl *et al* 2023 *Nanotechnology* **34** 175706

View the [article online](#) for updates and enhancements.

You may also like

- [\(Invited\) Effect of Junction Resistance on the Percolation Conductivity of Metal Nanowire Networks for Transparent Conductors](#)
Shreshtha Mishra, Ying Xue, Nicholas Fata et al.
- [Uniformity improvement of Josephson-junction resistance by considering sidewall deposition during shadow evaporation for large-scale integration of qubits](#)
Tsuyoshi Takahashi, Norinao Kouma, Yoshiyasu Doi et al.
- [Metal silicide nanowires](#)
Lih-Juann Chen and Wen-Wei Wu



EDINBURGH INSTRUMENTS

WORLD LEADING MOLECULAR SPECTROSCOPY SOLUTIONS

edinst.com

The advertisement features a red background with the Edinburgh Instruments logo on the left, which consists of a circular pattern of white dots. In the center and right, several pieces of laboratory equipment are displayed, including a spectrometer labeled 'FSS' and another labeled 'FLS 1000'. The text 'WORLD LEADING MOLECULAR SPECTROSCOPY SOLUTIONS' is written in white, bold, uppercase letters. The website 'edinst.com' is shown in a white box in the bottom right corner.

Influence of tin oxide decoration on the junction conductivity of silver nanowires

Lilian Maria Vogl¹ , Violetta Kalancha², Peter Schweizer¹,
Peter Denninger¹ , Mingjian Wu¹ , Christoph Brabec²,
Karen Forberich^{2,3} and Erdmann Spiecker¹ 

¹Institute of Micro- and Nanostructure Research (IMN), Center for Nanoanalysis and Electron Microscopy (CENEM), Interdisciplinary Center for Nanostructured Films (IZNF), Friedrich-Alexander-Universität Erlangen-Nürnberg, Germany

²Institute Materials for Electronics and Energy Technology, Friedrich-Alexander-Universität Erlangen-Nürnberg, Germany

³Helmholtz Institute Erlangen-Nürnberg for Renewable Energy (IEK-11), Erlangen, Germany

E-mail: Erdmann.Spiecker@fau.de

Received 15 November 2022, revised 13 December 2022

Accepted for publication 17 January 2023

Published 13 February 2023



CrossMark

Abstract

Flexible electrodes using nanowires (NWs) suffer from challenges of long-term stability and high junction resistance which limit their fields of applications. Welding via thermal annealing is a common strategy to enhance the conductivity of percolated NW networks, however, it affects the structural and mechanical integrity of the NWs. In this study we show that the decoration of NWs with an ultrathin metal oxide is a potential alternative procedure which not only enhances the thermal and chemical stability but, moreover, provides a totally different mechanism to reduce the junction resistance upon heat treatment. Here, we analyze the effect of SnO_x decoration on the conductance of silver NWs and NW junctions by using a four-probe measurement setup inside a scanning electron microscope. Dedicated transmission electron microscopy analysis in plan-view and cross-section geometry are carried out to characterize the nanowires and the microstructure of the junctions. Upon heat treatment the junction resistance of both plain silver NWs and SnO_x-decorated NWs is reduced by around 80%. While plain silver NWs show characteristic junction welding during annealing, the SnO_x-decoration reduces junction resistance by a solder-like process which does not affect the mechanical integrity of the NW junction and is therefore expected to be superior for applications.

Keywords: electron microscopy, nanowires, electrical measurements, junctions


(Some figures may appear in colour only in the online journal)

1. Introduction

Within the last years much effort has been put in optimizing the performance of nanowire (NW) based electrodes. Recently, efficiency records of nanowire based organic solar cells have been reported [1] and the application in flexible displays shows promising developments [2]. NWs are also

used in modern field effect transistors as reliable interconnects [3] to overcome scaling limitations [4]. All these devices have in common exceptional electrical properties due to the nanostructure.

A prerequisite for the use of NWs in functional devices is a reliable synthesis. The successful upscaling of one-pot synthesis methods enabled a high through-put production of uniformly shaped metal NWs, like five-fold twinned silver NWs with huge aspect ratio [5, 6]. Percolated networks of silver NWs can serve as transparent electrodes, which combine high optical transmission with low sheet resistance [7] and flexible behaviour [8, 9]. The overall electrode

 Original content from this work may be used under the terms of the [Creative Commons Attribution 4.0 licence](https://creativecommons.org/licenses/by/4.0/). Any further distribution of this work must maintain attribution to the author(s) and the title of the work, journal citation and DOI.

conductivity is governed by the electrical conductance of the single NWs and the resistance arising from the NW junctions [10, 11]. While the electrical conductance of single NWs are largely determined by intrinsic material properties, the amount of junctions translates directly into the network resistance. Therefore, reducing the number of junctions and enhancing the contact interface between the single NWs leads to an improved network conductivity. Joining of individual NWs via electrical [12], thermal [13] or plasmonic [14] heating enhances the contact interface by creating welding points [15] which significantly decrease the junction resistance. Despite the promising electrical properties of silver NWs, their usage is still limited by their long-term stability [16, 17]. The degradation caused by atmospheric moisture is well-known from the bulk-material [18] and becomes even more significant on small scales [19]. To preserve the silver NWs, subsequent coating strategies have been developed [20–22]. By adapting a one-pot synthesis, the surface of the NWs can be directly modified [23]. A complete encapsulation of the NWs leads to a high junction resistance, as the metal cores are separated by the protective shell and the creation of welding structures is hindered. Nevertheless, the decoration of the NW surface allows creating conductive electrodes with high chemical and thermal stability [24]. Moreover, the optical properties of the NWs are maintained or can be even tailored by surface decoration, which is interesting for optoelectronic devices where the NW network is used as a electrode as well as plasmonic waveguide [25].

In this work, we analyze the effect of partial tin oxide encapsulation on the electrical performance of silver NWs (SnO_x/Ag NWs) and their junctions compared to conventional five-fold twinned Ag NW. The four-point measurement setup based on micromanipulators inside the scanning electron microscope (SEM) allows for a precise contacting of single NWs and NW junctions. The microstructure at the junctions is analyzed by high-resolution and analytical transmission electron microscopy (TEM). The reference silver NWs show the expected welded structure after annealing with resulting reduced junction resistance. Interestingly, the SnO_x -decorated NWs do not show characteristic welding after heating, but the junction resistance decreases in a similar manner, which can be explained by a solder-like process enabled by the partial tin oxide encapsulation.

2. Methods and materials

2.1. Nanowire synthesis

Five-fold twinned silver NWs were synthesized by the polyol method. The procedure is based on previous work [23] with slightly modified parameters. Polyvinylpyrrolidone (PVP/0.417g) was added to Ethylene glycol (EG/40 ml) in a round-bottom flask (70 °C/1–2 h) until complete dissolution. After cooling to 25 °C, tetrabutylammonium chloride (TBAC/0.072g) solved in EG (10 ml) and Silver Nitrate (AgNO_3 /0.425g) was added. After mixing (15 min) the solution is overflowed to 100 ml autoclave and heated up to 140 °C for 20 h without

stirring. The final solution containing NWs was purified by centrifugation (2500 rpm/1 h/dilution with water). Residuals from the reaction were diluted by washing with NH_4OH (100 μl). For the SnO_x -decoration, Tin (II) 2-ethyl hexanoate (50 μl) was added to the NW dispersion in ethanol (30 ml). After mixing (15 min) the solution was kept at room temperature (2h). Then the solution was centrifuged and finally dispersed in ethanol.

2.2. Structural characterization

Samples for structural characterization using SEM were drop-casted on Si/ SiO_x substrate, while those for plan-view TEM studies were drop-casted on lacey carbon TEM grids. Cross-sectional samples of NWs and their junctions were prepared using focused ion beam (FIB) lift-out routines. SEM and FIB were performed on a ThermoFischer Scientific (TFS) Helios 660 Dual-beam instrument, (here with necessary parameters). TEM and STEM investigations were performed either on double Cs-corrected TFS Titan Themis microscopes operated at 300 kV or on a TFS Spectra 200 X-CFEG microscope operated at 200 kV. On both TEM platform, high performance Super-X energy dispersive x-ray spectroscopy (EDXS) system are equipped and used to map the elemental distribution. The EDXS datasets are evaluated with Velox software using standard k-factor method as implemented. In all SEM and TEM experiments, electron beam dose were carefully controlled and beam induced effects were evaluated and minimized.

2.3. Electrical measurements

The electrical measurements are performed via four-point testing inside the SEM. The NWs are drop-casted on insulating substrates. Subsequently the sample was annealed on a heating plate for 5 min at 300 °C. Figure 1(d) shows some representative close-up SEM images of heat-treated SnO_x/Ag NWs, which we chose for electrical characterization. To contact the NWs, four independent Kleindiek micromanipulators (MM3A-EM) equipped with low-current measurement (LCMK) kits are used. Commercial platinum tips with a tip radius of 50 nm allow contacting single NWs precisely. The tips are linearly arranged along the NW and current is applied between the outer tips with a connected Keithley 6485. The voltage drop between the inner tips is measured and used to calculate the resistance of the NW. During measurement, the electron beam is switched off. The maximum applied current density was $3.8 \times 10^8 \text{ A m}^{-2}$, which is much lower than the reported value for failure [26]. For resistance measurements of NW junctions two tips are placed on each side of the junction, as described in more detail below.

3. Results

3.1. Microstructure and thermal stability of the NWs and junctions

Figure 1 shows typical SnO_x/Ag NWs characterized by TEM and SEM, revealing key features of the sample structure. In

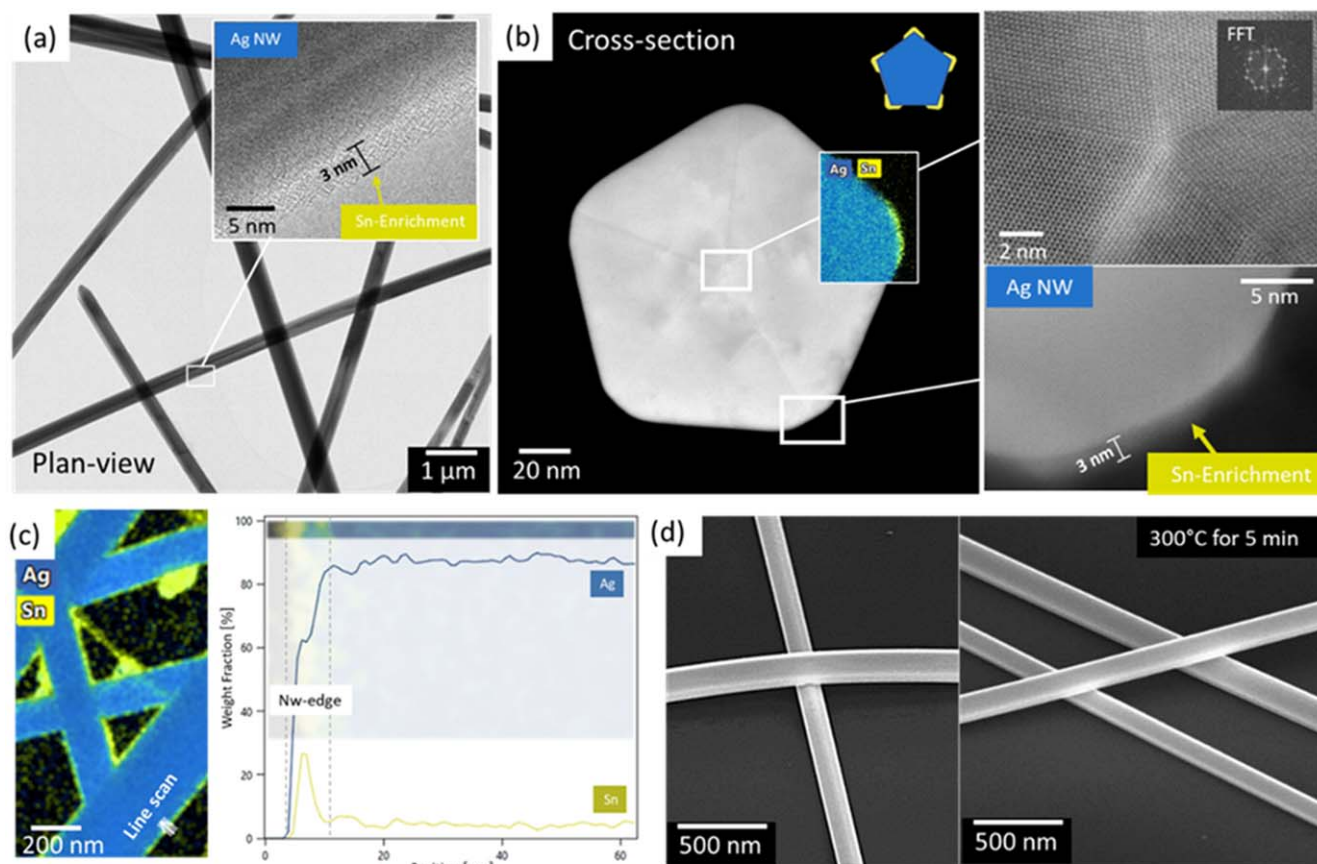


Figure 1. Microscopic characterization of SnO_x -decorated silver NWs. (a) Plan-view TEM revealing an amorphous shell (3 nm) at the nanowire edge. (b) TEM cross-section. Five-fold twinned structure with edge decoration (inset: schematic). EDX mapping with Sn and Ag signal. (c) EDX mapping and line scan confirming tin enrichment near the NW edge. (d) SnO_x/Ag NW junctions before and after heat treatment (300 °C for 5 min). No characteristic welding is observed.

plan-view TEM imaging (figure 1(a)), the NWs have a uniform appearance with a 3–5 nm amorphous shell at the edge. The NWs possess a characteristic pentagonal cross-section resulting from the five-fold twinned microstructure [27]. Figure 1(b) shows a NW cross-section with an elemental mapping (using energy dispersive x-ray spectroscopy, EDX) of one corner as inset. The amorphous layer shows the presence of Sn (yellow) adjacent to the Ag (blue) of the NW core. The observations are consistent with plan-view EDX analysis displayed in figure 1(c).

Near the edges a clear Sn signal is detected. Due to the pentagonal cross-section, in plan-view one of the corners of the pentagon is always visible in projection on either side of the wires. The Sn-treatment during the one-pot synthesis introduces the formation of an amorphous SnO_x layer at the silver NW edges (corners in cross-section) which obviously act as heterogeneous nucleation sites for the layer growth.

Literature indicates an increased temperature stability of silver NWs caused by a SnO_2 shell [16]. In contrast to covering the whole NW with a continuous shell, our process results in a partial coverage or decoration of the NW with amorphous SnO_x preferentially located at the NW edges. The conductivity of nonstoichiometric tin oxide films generally depends on various parameters such as annealing time, defects and O/Sn ratio [28]. With partial SnO_x encapsulation,

we aim to enhance the stability of the silver NWs against degradations, while maintaining the electrical and optical properties of Ag NW for applications as electrode.

Figure 2 compares qualitatively the stability of Ag NWs and SnO_x -decorated NWs at elevated temperatures. Already after 5 min of heating, the pristine NWs weld at the junctions, whereas the decorated NWs do not show such a junction-welding. After 30 min, the Ag NWs decompose preferentially at the welded junctions, which would cause a complete electrical failure in application. In comparison, the decorated NWs are still connected and despite particle formation, no further decomposition is observed. Even after 45 min the junctions of SnO_x -decorated Ag NWs are still intact whereas extensive degradation is observed in the case of the plain Ag NWs. Therefore the decoration of the NW not only affect the junction resistance (as described below), but also increase the stability against thermal degradation. For our study, we chose the parameters for the temperature treatment based on previous work [23].

3.2. Resistance of junctions of Ag NW and SnO_x/Ag NW

To calculate the resistance of a NW junction, the resistance and resistivity of a single NW have to be analyzed and compared to the bulk material firstly. In order to do so, four

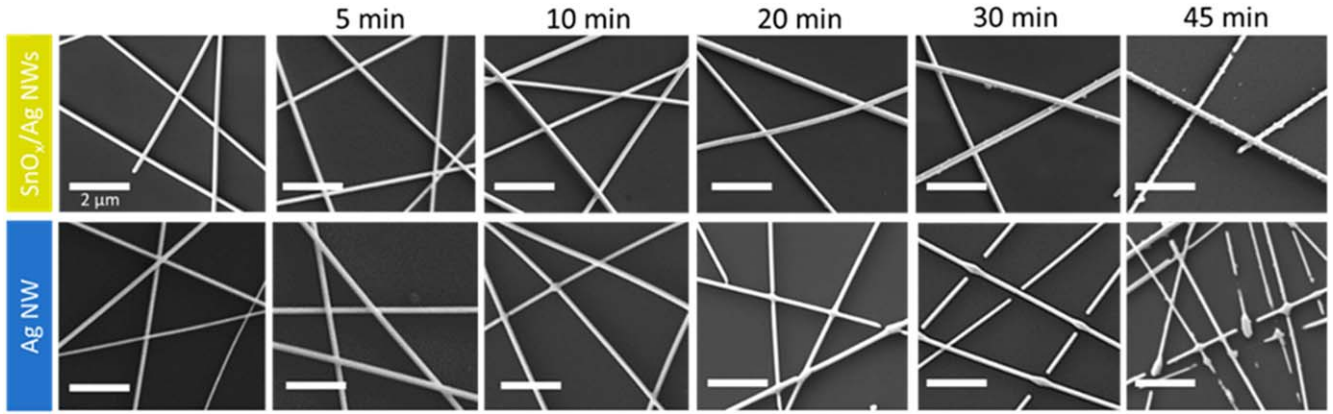


Figure 2. Comparison of SnO_x/Ag NWs and Ag NWs heated at 150 °C under atmospheric conditions for different times (5–45 min). After 30 min of heating, the Ag NWs decompose which would lead to an electrical break-down in devices. The SnO_x/Ag NWs show a higher stability against thermal degradation.

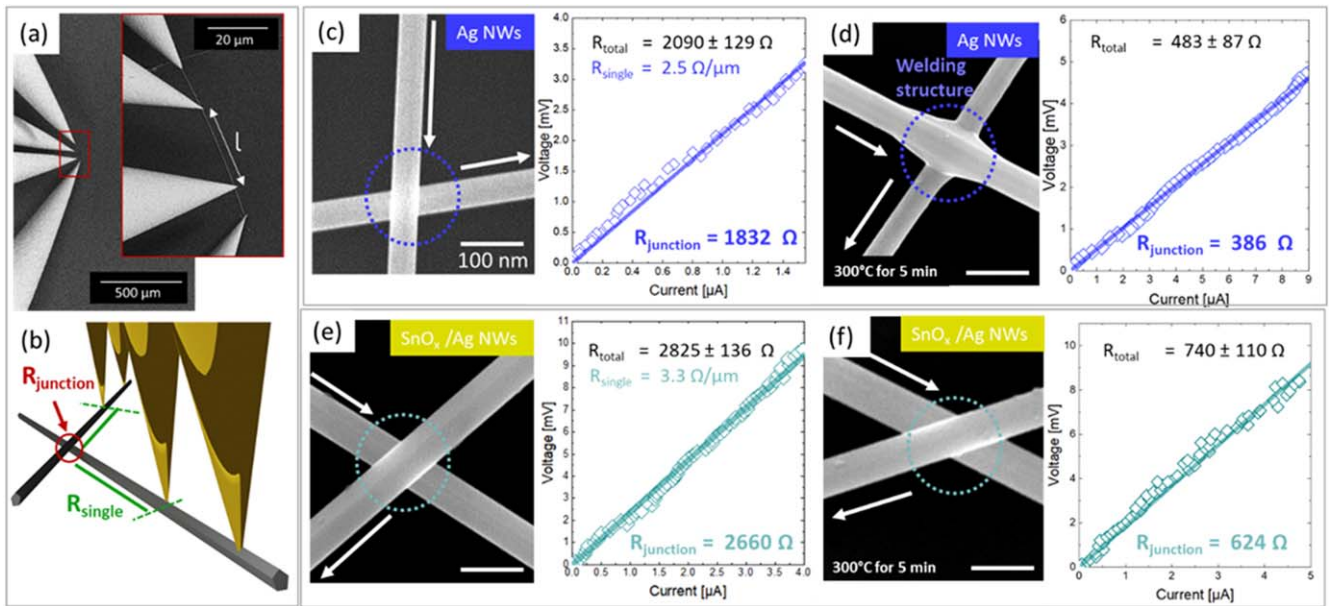


Figure 3. (a) SEM image of the linearly arranged four-point measurement setup. (b) Schematic of the four-point measurement across single NW junctions. SEM image and corresponding UI-curve for (c) as-prepared silver NW, RT (d) silver NWs, heated at 300 °C for 5 min (e) as-prepared SnO_x/Ag NWs, RT, and (f) SnO_x/Ag NWs, heated at 300 °C for 5 min.

tips are linearly arranged on a NW (figure 3(a)). The resistance of the NW R_{singleNW} is given by the ratio of the measured voltage U to the applied current I , which is used to determine the resistivity:

$$\rho = R \cdot A/l, \quad (1)$$

in which A is the area of NW cross-section and l the distance between the two inner tips. In literature, single penta-twinned silver NW have already been measured resulting in resistivity values in the range of $\rho_{\text{NW}} = 4.5\text{--}8.7 \times 10^{-8} \Omega\text{m}$ [24], slightly larger than the reported values of bulk silver $\rho_{\text{bulk}} = 1.6 \times 10^{-8} \Omega\text{m}$ [29]. With our setup, we measured the resistance per μm of the reference silver NW and obtained a value of $R_{\text{singleNW}}(\text{Ag}) = 2.5 \Omega \mu\text{m}^{-1}$. With the measured NW diameter of 65 nm a resistivity of $\rho_{\text{NW}}(\text{Ag}) = 2.4 \times 10^{-8} \Omega\text{m}$ is obtained in good agreement with literature. In general, bulk silver gets easily tarnished under atmosphere by sulphur

containing gases [30]. Despite the low concentration in normal atmosphere [18], the reaction causes severe difficulties in electrical applications of silver NWs. The resistivity of silver sulfide amounts to $\rho_{\text{silver sulfide}} = 10^{-12} \Omega\text{m}$ [31] which is orders of magnitude higher than that of silver. By decreasing the size and going to small scales, the corrosive reaction is even more dominant due to the higher surface-to-volume ratio. As shown by our recent work, an amorphous SnO_x encapsulation protects the silver NW from such a degradation [23]. The resistance per μm of the SnO_x-decorated NW is $R_{\text{singleNW}}(\text{SnO}_x/\text{Ag}) = 3.3 \Omega \mu\text{m}^{-1}$. With the measured cross-sectional area this translates to only a slightly higher resistivity of $\rho_{\text{NW}}(\text{SnO}_x/\text{Ag}) = 3.8 \times 10^{-8} \Omega\text{m}$ compared to plain Ag NWs. Despite the slightly decreased electrical performance, the decorated NWs show high potential as electrode material due to the enhanced stability against thermal degradation, as demonstrated in figure 2.

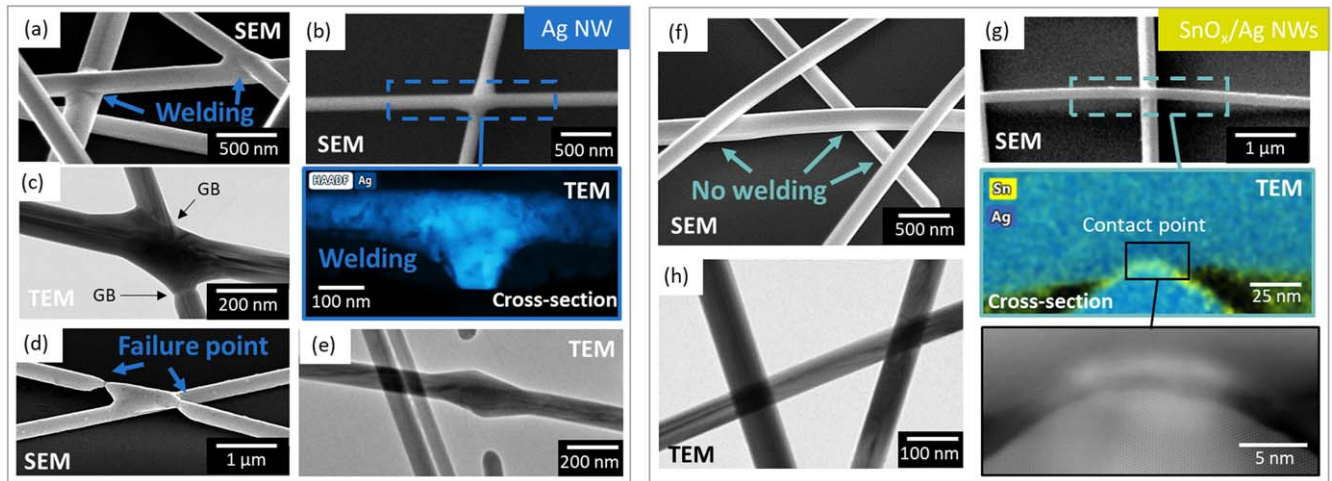


Figure 4. Overview of SEM and TEM studies of NW junctions showing representative images of junctions for pristine silver NWs (a)–(e) and for SnO_x-decorated silver NWs (f)–(h) after heat treatment at 300 °C for 5 min (a) Weld structures in SEM. (b) SEM image of a junction used for TEM cross-section preparation. HAADF/EDX (Ag) mapping in cross-section. (c) Weld structure in TEM plan-view. GB: Grain boundaries near the junction. (d) SEM image (tilted view) showing failure points near the junction. (e) TEM plan-view showing loss of interconnectivity near a NW junction. (f) SEM image of nanowire junctions of SnO_x-decorated NWs after heat treatment. No welding is observed. (g) SEM image of junction for TEM cross-section preparation. EDX mapping (Sn/Ag) in cross-section. HAADF image of contact point. (h) TEM plan-view image of junctions.

To characterize the resistance arising from NW junctions, the arrangement of the tips has to be adapted. The schematic in figure 3(b) gives an overview of the electrical measurement across a single NW junction. Two sufficiently long NWs showing a defined crossing point/junction are chosen for measurement. Two contact tips are placed on either side of the junction, meaning that the voltage drop across the junction is measured. Therefore, the measured resistance R_{total} includes the resistance arising from the single NWs R_{singleNW} and the resistance arising from the NW junction R_{junction} in a serial connection:

$$R_{\text{total}} = R_{\text{junction}} + R_{\text{singleNW}}. \quad (2)$$

Figures 3(c) and (d) show the recorded UI-curves and the corresponding SEM image of the reference silver NW junctions. Without any temperature treatment, the junction resistance shows a very high value of $R_{\text{junction}}(\text{Ag, RT}) = 1832 \Omega$ indicating a poor electrical contact. After heat treatment the NW junctions show characteristic welding resulting in a decrease of the junction resistance by 79% to $R_{\text{junction}}(\text{Ag, Temp.}) = 386 \Omega$. A similar behaviour is observed for the SnO_x/Ag NWs, displayed in figures 3(e) and (f). The measured junction resistance of the drop-casted NWs shows a high value of $R_{\text{junction}}(\text{SnO}_x/\text{Ag, RT}) = 2660 \Omega$, higher than that of bare Ag NWs junction, as expected. After heat treatment, the resistance of the junction decreases by about 77% to $R_{\text{junction}}(\text{SnO}_x/\text{Ag, Temp.}) = 624 \Omega$. In contrast to the heat-treated reference silver junction, the SnO_x-decorated junction does not show a characteristic heat-induced weld structure at the junction. Nevertheless, the temperature treatment shows the same positive effect on the conductance of the NW junction, suggesting improved electric conductance mechanism other than welding.

To elucidate the structural differences, detailed structure analysis was carried out at the junctions of Ag NWs and

SnO_x/Ag NWs. Figure 4 is an overview of some representative SEM and TEM (plan-view/cross-section) images of heat-treated NW junctions. During heat treatment, the overlapping silver NWs merge with each other, creating a continuous internal crystalline microstructure. Figure 4(a) shows such junction welding in SEM and figure 4(c) displays two welded NWs in TEM plan-view. In general, interfaces act as barrier for the electron pathway [32, 33] and therefore increase the resistance. Without welding, the electrons have to travel through the NW-NW interface and the junction resistance is high. Heat treatment improves the interface of the overlapping NWs. Figure 4(b) shows the cross-section of a characteristic welded structure in TEM.

This explains the significant reduction of junction resistance by ~79%. However, redistribution of material near the junction (via surface diffusion [34]) results in the creation of mechanically vulnerable failure points, due to mass transport close to the junction points (see figures 4(d) and (e)) [35]. In contrast, the SnO_x-decorated NWs do not show such a material redistribution upon thermal annealing. Figures 4(f) and (h) depict typical SEM and TEM images of SnO_x/Ag NW junctions. During heat treatment the geometry of the NWs is retained. Due to the absence of NW welding Ag mass transport is suppressed thus reducing the number of mechanical failure points. Still the electrical performance of NW junctions is significantly improved as shown by the electrical measurements. A TEM image of a NW junction in cross-section is displayed in figure 4(g). At the contact point, the amorphous Sn enriched layer is still visible as an inter-layer between the two NWs (see EDX mapping and HAADF image). This clearly shows that the lower junction resistance cannot be explained in the same way as for the welded Ag NWs without SnO_x decoration. Rather a different process

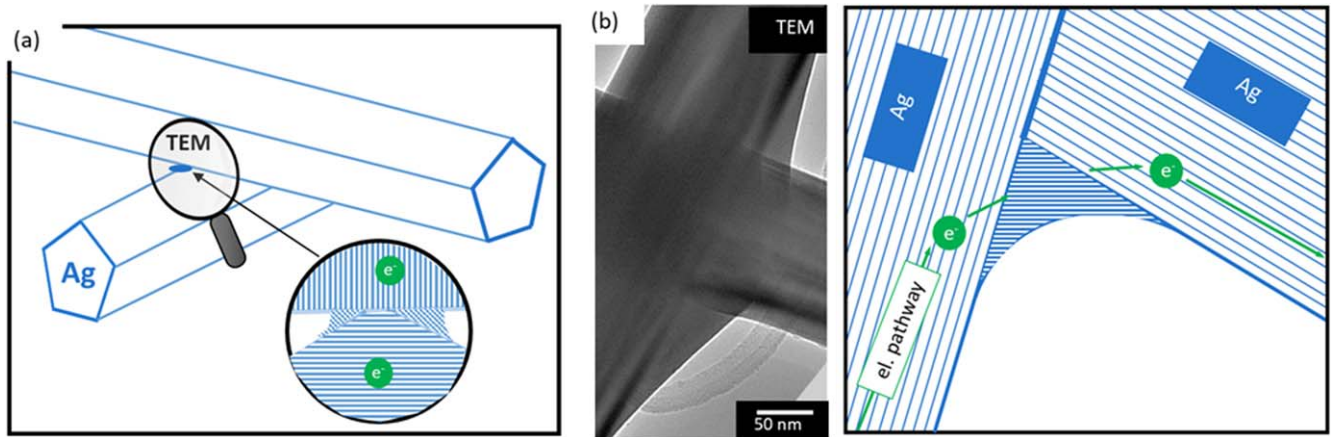


Figure 5. Schematic illustration to describe the junction structure of Ag NWs after heat treatment based on TEM investigations. (a) Two welded Ag NWs (b) TEM plan-view of junction welding.

involving the presence of Sn at the interface must be active. A possible mechanism based on our observations will be discussed in the following section.

4. Discussion

Compared to the literature [10, 36, 37], our measured values for the junction resistance are relatively high. Nevertheless, the intrinsic resistivity of the NWs is in good agreement [38]. We attribute this to differences in heat treatment, choice of substrate and variations in wire synthesis. Despite the higher absolute junction resistance values, the relative effect of the heat treatment is consistent. After heat treatment, the reference NWs and the SnO_x -decorated NWs show comparable improvement of electrical behaviour. However, the contact points at the NW junction indicate different mechanisms for both wire types.

Figures 5 (a) and (b) illustrate schematically the observed junction structures based on TEM investigations of pristine silver NWs. Upon heat treatment, contacting silver NWs are welded together. In literature they proposed a thermally induced welding mechanism involving surface diffusion and epitaxial regrowth of silver at the NW junction [34, 39]. Garnett *et al* showed that the epitaxial recrystallization is spatially limited to the junction [39]. The NW near the junction maintained its original orientation, leading to distinct grain boundaries next to the junction [39], also visible in figure 4(c).

Our measurement shows that the weld structure provides an electrical pathway which reduces the junction resistance by 79% compared to the NW-NW contact before temperature treatment. However, the junction resistance is still higher than what would be expected for a purely epitaxial interface. This might be explained by the presence of the induced grain boundaries and the associated reduction of the cross-section, see figure 4(c). In addition, impurities incorporated into the weld can increase the resistance further [36].

For the SnO_x -decorated junctions, welding is suppressed and a solder-like process based on the solder agent SnO_x is induced. Figures 6(a) and (b) illustrates the proposed mechanism based on TEM investigations. In contrast to welding, soldering is generally based on the creation of a joint by using a solder material which has a much lower melting temperature compared to the adjoining metals [40]. Tin- and silver-rich compounds are used as solder material for micro- [41] and nano-joints [42] as they show advantageous properties regarding the mechanical reliability [43] and solderability [44]. In our case, the joint is not created by melting the solder, but by partial crystallisation based on tin-enriched compounds.

After heat treatment, small crystalline particles are observed on the NW surface. In TEM, we see characteristic particle agglomeration near NW junctions (see figures 6(b) and (c)). The crystalline particles are embedded in an amorphous matrix and provide the connection between the two NWs. The overall SnO_x -decoration is still amorphous and no continuous crystalline tin oxide is observed. One reason for the positive effect on the junction resistance after heating can be the creation of crystalline silver-tin particles in combination with the changing conductivity of the non-stoichiometric tin oxide. The structure of the amorphous SnO_x layer remains unchanged, however, the oxygen loss results in an increased density of Sn^{2+} sites, which increases the overall conductivity [28]. Figure 6(d) compares EDX line scans of SnO_x -decorated NWs before and after heat treatment. We observe a clear Sn-signal and an overall oxygen depletion after heat treatment. The partial SnO_x -encapsulation can be seen as solder agent, which facilitates the electron mobility at the NW junctions and enables the creation of crystalline particles. During four-point probing of the single NW, the electric current is likely to transport within the silver NW, as it is, compared to the amorphous layer, the pathway of least resistance. By measuring across a junction, the current has to pass the NW-NW interface. A conductive interlayer enhances the electrical contact similar to a solder-joint without the need of a weld structure. The absence of direct welding of the silver cores has the advantage that surface diffusion of silver is suppressed which reduces the formation

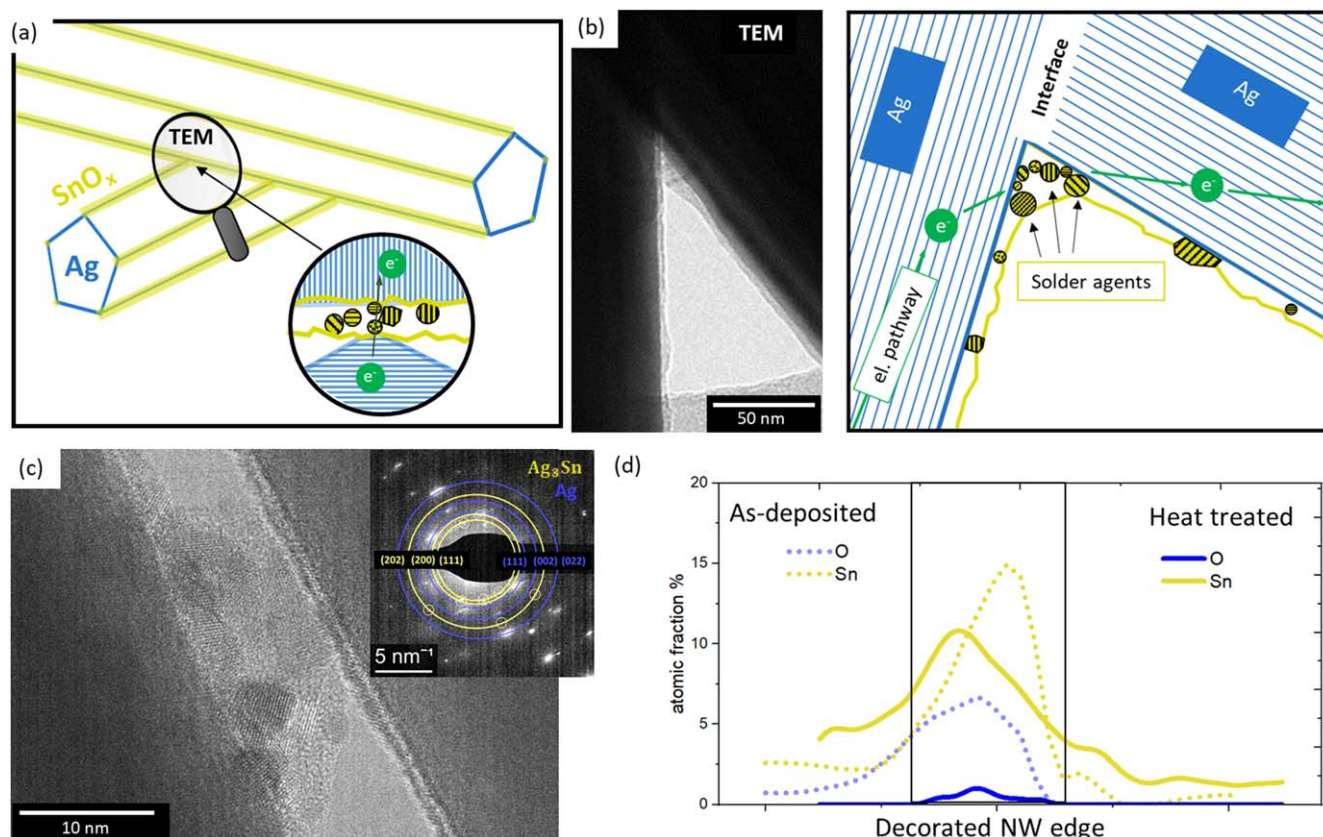


Figure 6. Schematic illustration to describe the junction structure of SnO_x -decorated silver NW after heat treatment based on TEM- images. (a) Two electrically connected SnO_x/Ag NWs without welding. (b) TEM plan-view image of the solder-like junction. (c) TEM image: SnO_x/Ag NWs connected via particles, which are embedded in an amorphous matrix. Inset: corresponding diffraction pattern (Ag, Ag_3Sn) (d) comparison of EDX line scans (Sn/O signal) of SnO_x/Ag NWs (as-prepared/heat treated).

of constrictions or other electrically and mechanically weak points at NW junctions (see also figures 1(d) and 4(f)).

5. Conclusion

We have investigated the effect of SnO_x -decoration on the conductivity of NW junctions by using a four-point measurement setup inside the SEM. Analysing single NW junctions opens up the opportunity to optimize NW electrodes and their post-treatments by knowing the behaviour on small scales. While pristine silver NWs show characteristic weld structures, the SnO_x -decorated NWs join in a different way. Cross-section analysis in TEM show the contact point at the NW junction. After heating, much of the amorphous SnO_x decoration is still present, however, the junction resistance reduces by around 80% (similar to the reference silver NWs). The increased conductivity cannot be explained by welding of the silver NWs. We present a possible explanation based on a silver-tin solder-like process. We believe that in future, the soldering process at the NW junctions can be used to create functional NW networks. Moreover, the chemical composition of the decoration can be adapted e.g. by using pure Sn to support the soldering process and to further stabilize nanoscale networks without affecting the optical and mechanical properties.

Acknowledgments

The authors gratefully acknowledge funding by the DFG through projects GRK 1896 and SFB 953.

Data availability statement

The data that support the findings of this study are available upon reasonable request from the authors.

ORCID iDs

Lilian Maria Vogl <https://orcid.org/0000-0001-8272-3146>
 Peter Denninger <https://orcid.org/0000-0002-2821-2799>
 Mingjian Wu <https://orcid.org/0000-0003-2113-0245>
 Erdmann Spiecker <https://orcid.org/0000-0002-2723-5227>

References

- [1] Wang Y, Chen Q, Zhang G, Xiao C, Wei Y and Li W 2022 Ultrathin flexible transparent composite electrode via semi-embedding silver nanowires in a colorless polyimide for

- high-performance ultraflexible organic solar cells *ACS Appl. Mater. Interfaces* **14** 5699–708
- [2] Nair N M, Khanra I, Ray D and Swaminathan P 2021 Silver nanowire-based printable electrochromic ink for flexible touch-display applications *ACS Appl. Mater. Interfaces* **13** 34550–60
- [3] Brunbauer F M, Bertagnolli E, Majer J and Lugstein A 2016 Electrical transport properties of single-crystal Al nanowires *Nanotechnology* **27** 385704
- [4] Wind L, Böckle R, Sistani M, Schweizer P, Maeder X, Michler J, Murphey C G E, Cahoon J and Weber W M 2022 Monolithic and single-crystalline aluminum–silicon heterostructures *ACS Appl. Mater. Interfaces* **14** 26238–44
- [5] Zhang Y, Guo J, Xu D, Sun Y and Yan F 2017 One-pot synthesis and purification of ultralong silver nanowires for flexible transparent conductive electrodes *ACS Appl. Mater. Interfaces* **9** 25465–73
- [6] Saw M J, Ghosh B, Nguyen M T, Jirasattayaporn K, Kheawhom S, Shirahata N and Yonezawa T 2019 High aspect ratio and post-processing free silver nanowires as top electrodes for inverted-structured photodiodes *ACS Omega* **4** 13303–8
- [7] Zhao Y, Fitzgerald M L, Tao Y, Pan Z, Sauti G, Xu D, Xu Y-Q and Li D 2020 Electrical and thermal transport through silver nanowires and their contacts: effects of elastic stiffening *Nano Lett.* **20** 7389–96
- [8] Wu B, Heidelberg A, Boland J J, Sader J E, Sun and Li 2006 Microstructure-hardened silver nanowires *Nano Lett.* **6** 468–72
- [9] Van De Groep J, Spinelli P and Polman A 2012 Transparent conducting silver nanowire networks *Nano Lett.* **12** 3138–44
- [10] Bellew A T, Manning H G, Gomes da Rocha C, Ferreira M S and Boland J J 2015 Resistance of single Ag nanowire junctions and their role in the conductivity of nanowire networks *ACS Nano* **9** 11422–9
- [11] Patil J J, Chae W H, Trebach A, Carter K-J, Lee E, Sannicolo T and Grossman J C 2021 Failing forward: stability of transparent electrodes based on metal nanowire networks *Adv. Mater.* **33** 2004356
- [12] Vafaei A, Hu A and Goldthorpe I A 2014 Joining of individual silver nanowires via electrical current *Nano-Micro Lett.* **6** 293–300
- [13] Lee J-Y, Connor S T, Cui Y and Peumans P 2008 Solution-processed metal nanowire mesh transparent electrodes *Nano Lett.* **8** 689–92
- [14] Ha J, Lee B J, Hwang D J and Kim D 2016 Femtosecond laser nanowelding of silver nanowires for transparent conductive electrodes *RSC Adv.* **6** 86232–9
- [15] Ding Y, Cui Y, Liu X, Liu G and Shan F 2020 Welded silver nanowire networks as high-performance transparent conductive electrodes: welding techniques and device applications *Appl. Mater. Today* **20** 100634
- [16] Zhao Y et al 2019 Protecting the nanoscale properties of Ag nanowires with a solution-grown SnO₂ monolayer as corrosion inhibitor *J. Am. Chem. Soc.* **141** 13977–86
- [17] Song T-B, Rim Y S, Liu F, Bob B, Ye S, Hsieh Y-T and Yang Y 2015 Highly robust silver nanowire network for transparent electrode *ACS Appl. Mater. Interfaces* **7** 24601–7
- [18] Franey J P et al 1985 The corrosion of silver by atmospheric sulfurous gases *Corrosion Science* **25** 133–43
- [19] Guan P et al 2021 Performance degradation and mitigation strategies of silver nanowire networks: a review *Crit. Rev. Solid State Mater. Sci.* **0** 1–25
- [20] Khan A, Nguyen V H, Muñoz-Rojas D, Aghazadehchors S, Jiménez C, Nguyen N D and Bellet D 2018 Stability enhancement of silver nanowire networks with conformal ZnO coatings deposited by atmospheric pressure spatial atomic layer deposition *ACS Appl. Mater. Interfaces* **10** 19208–17
- [21] Göbelt M, Keding R, Schmitt S W, Hoffmann B, Jäckle S, Latzel M, Radmilović V V, Radmilović V R, Spiecker E and Christiansen S 2015 Encapsulation of silver nanowire networks by atomic layer deposition for indium-free transparent electrodes *Nano Energy* **16** 196–206
- [22] Aghazadehchors S, Nguyen V H, Munoz-Rojas D, Jiménez C, Rapenne L, Nguyen N D and Bellet D 2019 Versatility of bilayer metal oxide coatings on silver nanowire networks for enhanced stability with minimal transparency loss *Nanoscale* **11** 19969–79
- [23] Kalancha V et al 2022 Overcoming temperature-induced degradation of silver nanowire electrodes by an Ag@SnOx core–shell approach *Adv. Electron. Mater.* **8** 2100787
- [24] Arefpour M, Almasi Kashi M and Bagheli M 2020 High chemical and thermal stability of Ag nanowire-based transparent conductive electrodes induced by electroless Ag nanoparticle decoration *Phys. Status Solidi a* **217** 1900957
- [25] Kim T, Kang S, Heo J, Cho S, Kim J W, Choe A, Walker B, Shanker R, Ko H and Kim J Y 2018 Nanoparticle-enhanced silver-nanowire plasmonic electrodes for high-performance organic optoelectronic devices *Adv. Mater.* **30** 1800659
- [26] Waliullah M and Bernal R A 2022 Current density at failure of twinned silver nanowires *Nanotechnology* **33** 305706
- [27] Niekief F, Spiecker E and Bitzek E 2015 Influence of anisotropic elasticity on the mechanical properties of fivefold twinned nanowires *J. Mech. Phys. Solids* **84** 358–79
- [28] Alterkop B, Parkansky N, Goldsmith S and Boxman R L 2003 Effect of air annealing on opto-electrical properties of amorphous tin oxide films *J. Phys. D* **36** 552–8
- [29] Matula R A 1979 Electrical resistivity of copper, gold, palladium, and silver *J. Phys. Chem. Ref. Data* **8** 1147–298
- [30] Huo Y, Fu S-W, Chen Y-L and Lee cc 2016 A reaction study of sulfur vapor with silver and silver–indium solid solution as a tarnishing test method *J. Mater. Sci., Mater. Electron.* **27** 10382–92
- [31] Hebb M H 1952 Electrical conductivity of silver sulfide *J. Chem. Phys.* **20** 185–90
- [32] Chawla J S, Gstrein F, O'Brien K P, Clarke J S and Gall D 2011 Electron scattering at surfaces and grain boundaries in Cu thin films and wires *Phys. Rev. B* **84** 235423
- [33] Bishara H, Ghidelli M and Dehm G 2020 Approaches to measure the resistivity of grain boundaries in metals with high sensitivity and spatial resolution: a case study employing Cu *ACS Appl. Electron. Mater.* **2** 2049–56
- [34] Radmilović V V, Göbelt M, Ophus C, Christiansen S, Spiecker E and Radmilović V R 2017 Low temperature solid-state wetting and formation of nanowelds in silver nanowires *Nanotechnology* **28** 385701
- [35] Hwang B, Shin H-A-S, Kim T, Joo Y-C and Han S M 2014 Highly reliable Ag nanowire flexible transparent electrode with mechanically welded junctions *Small* **10** 3397–404
- [36] Selzer F, Floresca C, Knepe D, Bormann L, Sachse C, Weiß N, Eychmüller A, Amassian A, Müller-Meskamp L and Leo K 2016 Electrical limit of silver nanowire electrodes: direct measurement of the nanowire junction resistance *Appl. Phys. Lett.* **108** 163302
- [37] Hu L, Kim H S, Lee J-Y, Peumans P and Cui Y 2010 Scalable coating and properties of transparent, flexible, silver nanowire electrodes *ACS Nano* **4** 2955–63
- [38] Bernal R A, Filleter T, Connell J G, Sohn K, Huang J, Lauthon L J and Espinosa H D 2014 *In situ* electron microscopy four-point electromechanical characterization of freestanding metallic and semiconducting nanowires *Small* **10** 725–33
- [39] Garnett E C, Cai W, Cha J J, Mahmood F, Connor S T, Greyson Christoforo M, Cui Y, McGehee M D and

- Brongersma M L 2012 Self-limited plasmonic welding of silver nanowire junctions *Nat. Mater.* **11** 241–9
- [40] Schwartz M M 2014 *Soldering: Understanding the Basics* (ASM International)
- [41] Tian Y, Ren N, Zhao Z, Wu F and Sitaraman S K 2018 Ag₃Sn compounds coarsening behaviors in micro-joints *Materials (Basel)* **11** 2509
- [42] Zhang H, Zhang J, Lan Q, Ma H, Qu K, Inkson B J, Mellors N J, Xue D and Peng Y 2014 Nanoscale characterization of 1D Sn-3.5 Ag nanosolders and their application into nanowelding at the nanoscale *Nanotechnology* **25** 425301
- [43] Chu K, Lee C, Park S-H and Sohn Y 2017 Effects of Ag addition and Ag₃Sn formation on the mechanical reliability of Ni/Sn solder joints *Microelectron. Reliab.* **75** 53–8
- [44] Chung C K and Tai S 2004 Evolution of Ag₃Sn during reflow soldering *IEEE Cat. No.04CH37543* **2** 116–20